ACS APPLIED NANO MATERIALS

www.acsanm.org

Article

Biocompatible Germanium-Doped Hydroxyapatite Nanoparticles for Promoting Osteogenic Differentiation and Antimicrobial Activity

Miloš M. Lazarević, Nenad L. Ignjatović, Qene Mahlet, Violet V. Bumah, Milena Radunović, Jelena Milašin, Dragan P. Uskoković, and Vuk Uskoković*

Cite This: https://doi.org/10.1021/acsanm.3c05974

Read Online

ACCESS | Metrics & More | Article Recommendations

ABSTRACT: Hydroxyapatite (HAp) has been the main protagonist in the quest for an ideal biomaterial for regenerative medicine over the last half a century. To control its properties, this material has commonly been doped with chemical elements other than its natural stoichiometric constituents: Ca, O, P, and H. Here, we report on the first analysis of the biological response to germanium-doped hydroxyapatite (Ge-HAp). Cytotoxicity, osteogenic differentiation induction, and colony formation potential were measured on dental pulp stem cells, while the antimicrobial effect was assessed against Gram-negative *Escherichia coli*, Gram-positive methicillin-resistant *Staphylococcus aureus* (MRSA), and *Candida albicans*. All analyses were run in comparison to Ge-free HAp. Cell viability was inversely dependent on the nanoparticle concentration and incubation time. Adding Ge to HAp reduced cell viability relative to HAp after 24−72 h incubation periods, but the effect was reversed after longer incubations, when the viability of cells treated with low doses of Ge-HAp exceeded that of HAp-treated cells and became comparable with control culture. Both HAp and Ge-HAp induced mineral formation in the cell culture, but the effect was more pronounced for Ge-HAp. Likewise, relative to both control cells and cells exposed to HAp, Ge-HAp upregulated the expression of all three osteogenic markers analyzed, namely, alkaline phosphatase, RUNX2, and osteocalcin, exerting the key influence on osteogenesis in its early, differentiation stage. The colony formation capacity of stem cells, however, was impaired by HAp and even more so by Ge-HAp. The antimicrobial effect was dependent on the microorganisms tested. Thus, whereas the antimicrobial activity was absent against *E. coli*, it was evident against MRSA and *C. albicans*. While the antibacterial activity against MRSA was weakened by the addition of Ge to HAp, the antimycotic activity against *C. albicans* was intensified with the addition of Ge. These findings demonstrate a significant potential of Ge-doped HAp nanoparticles in regenerative medicine due to their pronounced biocompatibility, osteoinductivity, and antimicrobial activity.

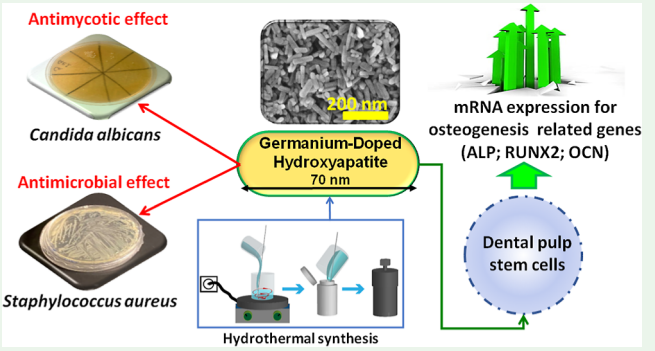

KEYWORDS: *antibacterial, antifungal, calcium phosphate, doping, flow cytometry, nanomedicine, tissue engineering*

INTRODUCTION

Regenerative medicine is a multidisciplinary area integrating science, technology, and clinical practice with the objective of regenerating malfunctioning tissues and organs in the human body. To this end, stem cells, that is, multipotent progenitor cells capable of differentiating into multiple phenotypic lineages, have played a pivotal role. Hematopoietic and mesenchymal stem cells (MSCs) are the types of primary adult stem cells that have been employed in regenerative medicine more than any other stem cells. The dental pulp is an excellent source of a particular form of MSCs known as dental pulp stem cells (DPSCs), the collection of which is noninvasive and simple after tooth extraction.[1−3]

The direct insertion of stem cells into the physiological areas of interest, however, does not always present a viable strategy because of the uncontrolled migration and differentiation of these cells. Studies have shown, for example, that only up to 5% of stem cells directly injected into a physiological area get retained locally after a few days, and less than 1% of them survive.[4] To control the migration and differentiation of stem cells more precisely in regenerative medicine, these cells are combined with various scaffolds and employed as such for the treatment of tissue defects. In such a way, the differentiation of stem cells into desired lineages can be controlled by the physicochemical properties of the matrix onto which they are

Received: December 12, 2023
Revised: March 12, 2024
Accepted: March 18, 2024
Published: April 5, 2024

Scheme 1. Hydrothermal Synthesis Procedure Implemented for the Preparation of Germanium-Doped Hydroxyapatite Nanoparticles

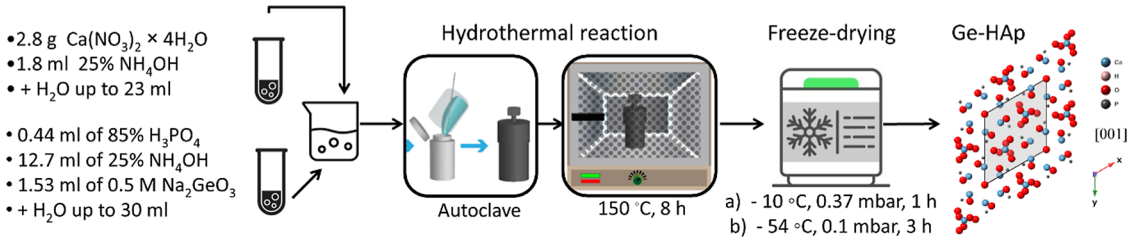

seeded. Such an approach has grown into a central paradigm in the field of tissue engineering. A recent literature review, for example, has demonstrated a promising early formation of new bone in preclinical animal experiments and concluded that DPSCs are a valuable resource for regenerative bone augmentation procedures.[5] The osteogenic differentiation of DPSCs on various scaffolds was evaluated on numerous other occasions previously.[6−8] One particularly interesting scaffold for bone tissue regeneration is hydroxyapatite (HAp).

Nanoparticulate calcium phosphates, especially HAp, have been the subject of numerous studies that evaluated their use in reconstructive and regenerative medicine.[9−11] Because HAp presents the synthetic analogue of biological apatite, most of the applications for various forms of HAp have been geared toward pharmacy, dentistry, and medicine. Decades of research on nanoparticulate HAp have made it possible to build a vast array of multifunctional materials with osteoconductive, osteoinductive, antibacterial, magnetic, and other important properties.[12−15] HAp particles have been shown to be appropriate for the culture of MSCs. In fact, the inclusion of HAp nanoparticles into human DPSC cultures mimics the actual architecture of boney tissues, allowing for the modulation of expression of osteogenic genes such as osteocalcin (OCN), osteonectin, and runt-related transcription factor 2 (RUNX2).[16] This type of culture has led to a higher expression of osteo-specific genes in a fibroblastic cell line such as C3H10T1/2, including alkaline phosphatase (ALP), type I collagen, and OCN, relative to cultures not supplemented with HAp.[17] Correspondingly, HAp particles ranging in size from 50 to 150 nm strongly enhance the osteogenic differentiation of human MSCs.[18]

Despite the sparse solubility of HAp, its ability to sustain high lattice strains and defect concentrations translates to a pronounced propensity for ion exchange. This capacity for foreign ion accommodation has led to over 60 years of application of HAp in chromatographic columns[19] and for environmental remediation.[20] More recently, HAp started to be doped with foreign ions in the effort to impart new properties to it.[21] Over the last couple of decades, doping HAp nanoparticles with different elements of the Periodic Table has grown into a mainstream strategy for influencing not only chemical and physical properties of this material but also its biological behavior.[21] Ion-doped HAp nanoparticles affect cell properties differently from their undoped counterparts, which is of importance for reconstructive and regenerative medicine.[21−23] Doping HAp nanoparticles with ions such as Mg^{2+}, Sr^{2+}, and Zn^{2+}, for example, enhances their antibacterial, osteointegrative, and other biological characteristics.[24] Likewise, cobalt-doped HAp nanoparticles exhibit an improved reparative capabilities in reconstruction of osteoporosis-damaged bone tissue relative to undoped HAp.[25] Finally, doping HAp nanoparticles with rare earth elements, such as gadolinium, samarium, europium, and others, has opened up the path for HAp to applications in multimodal imaging.[26,27]

In our earlier work from 2022, we reported on the first synthesis and physicochemical characterization of HAp doped with germanium (Ge^{4+}) ions.[28] There are multiple ionic forms in which Ge can be introduced to HAp, including both cationic and anionic. Among all of them, we opted for the introduction of Ge in the form of germanate ions, GeO_3^{2-}, which replace phosphate groups in the crystal structure of HAp. Given that novel forms of ion-substituted HAp are being produced largely for biological purposes, it is worthwhile to consider what biological features the presence of Ge may confer to HAp. Germanium, first, has no known biological functions. Even though it is a nontoxic element[29] with anticancer, antiviral, antiaging, and anti-inflammatory properties,[30] its biomedical applications have been limited. In this study, we synthesized Ge-doped hydroxyapatite (Ge-HAp) and used it as a matrix for DPSCs. In particular, one aim of this study was to investigate the effect of Ge-HAp nanoparticles on viability, differentiation, and colony formation potential of DPSCs, alongside assessing their uptake by these cells. In addition, the antibacterial activity of Ge-HAp was tested against *Escherichia coli* and methicillin-resistant *Staphylococcus aureus* (MRSA) in vitro. Furthermore, the fungicidal potential of Ge-HAp against *Candida albicans* was determined. In order to assess the effect of the doping on the biological properties analyzed, all analyses were performed in comparison with HAp that was not doped with Ge.

EXPERIMENTAL SECTION

Synthesis of HAp and Ge-HAp. A previously developed procedure[26] was adapted for the synthesis of HAp and Ge-HAp. For that purpose, two basic solutions were prepared, one containing Ca^{2+} ions and another containing PO_4^{3-} ions (Scheme 1). The former solution was prepared by dissolving 2.8 g of $Ca(NO_3)_2 \times 4H_2O$ (Sigma-Aldrich, Germany) and 1.8 mL of 25% NH_4OH in 11 mL of distillated water and then adding water up to the total volume of 23 mL. The latter solution was prepared by adding 0.44 mL of 85% H_3PO_4, 1.2 mL of 25% NH_4OH, and 1.53 mL of 0.5 M aqueous solution of Na_2GeO_3 to 9.2 mL of distilled water and then adding water up to the total volume of 18.5 mL and 25% NH_4OH up to the total volume of 30 mL. After preheating to 50 °C, the second solution was added dropwise to the first solution as it was agitated with a magnetic stir bar. The resulting 70 mL of the colloidal suspension was transferred to a 100 mL Teflon-lined stainless-steel autoclave, in which the hydrothermal reaction was performed, at 150 °C for 8 h. After the given time and cooling, the sol was centrifuged, washed multiple times until pH 7 was attained. Finally, the obtained powder was subjected to two-step lyophilization, first at −10 °C and 0.37 mbar for 1 h, and then at −54 °C and 0.1 mbar for 3 h.[28]

Materials Characterization. A Carl Zeiss ULTRA Plus microscope was used to perform field-emission scanning electron microscopy (SEM). This analysis was carried out at an electron

https://doi.org/10.1021/acsanm.3c05974
ACS Appl. Nano Mater. XXXX, XXX, XXX−XXX

acceleration voltage of 3 kV and a working distance of 3.9 mm. Fourier transform infrared (FTIR) measurements were performed on a Thermo Scientific Nicolet iS10 spectrometer equipped with an attenuated total reflection accessory. The spectral range in which FTIR spectra were recorded was 400−4000 cm^{-1}.

Isolation of DPSCs. Semi-impacted wisdom teeth from three systemically healthy patients were used for DPSC isolation. Atraumatic tooth extraction was performed at the Clinic for Oral Surgery, School of Dental Medicine, University of Belgrade, Belgrade, Serbia, after having obtained a written informed consent form. The study was approved by the Ethics Committee and Review Board of the School of Dental Medicine (Protocol no. 36/2). Teeth were immediately transported to the laboratory and further processed under sterile conditions. Teeth surfaces were thoroughly rinsed with phosphate buffered saline solution (Thermo Fisher Scientific, Waltham, MA, USA), and DPSCs were isolated and characterized as previously described.[31,32] Briefly, the dental pulp was extracted with an endodontic instrument after having exposed the pulp chamber by crushing the tooth with a sterile clamp. Tissues were cut into 1 mm^3 pieces and transferred into culture medium [Dulbecco's Modified Eagle Medium (DMEM) supplemented with 10% fetal bovine serum (FBS) and 1% antibiotic-antimitotic solution (all from Thermo Fisher Scientific, Waltham, MA, USA)]. The cells were maintained at 37 °C in a humidified atmosphere containing 5% CO_2. The culture medium was changed every 2−3 days. Cell cultures were passaged after reaching 80% confluence. The assays were done on third-passage cells.

Flow Cytometry. For the flow cytometry analysis of the nanoparticle uptake, DPSCs were plated in six-well plates (10^6 cells/mL) in DMEM supplemented with 10% FBS and 1% antibiotic-antimycotic solution (all from Thermo Fisher Scientific, Waltham, MA, USA). Cells were incubated for 24 h without Ge-HAp and then treated with different concentrations of Ge-HAp nanoparticles for 24 h. The cells were then washed three times for 5 min each with phosphate-buffered saline (PBS) and trypsinized while still in the proliferative growth phase, centrifuged, resuspended in 1 mL of cold PBS with 10% FBS, and immediately analyzed. A BD FACSMelody (BD Biosciences, San Jose, CA, USA) flow cytometer containing a 488 nm laser, forward light scatter (FSC) diode detector, photomultiplier tube side light scatter (SSC) detector, and BD FACSChorus Software were used in the study. Because the flow rate affects these measurements, the latter were always performed at low flow rates. The cytometer was set up to measure the SSC logarithmically and FSC linearly. The highest dose of Ge-HAp nanoparticles (5 mg/mL) was run first to set the range for the maximum SSC signal and the minimum FSC signal.[33]

MTT Assay. MTT assay was done according to the ISO10993-5 standard. Five thousand DPSCs were seeded onto a 96-well plate. After 24 h, 100 μL of DMEM supplemented with 10% FBS and 1% antibiotic-antimycotic solution (all from Thermo Fisher Scientific, Waltham, MA, USA) (pH 6.9 to 7.3) supplemented with 5, 2.5, 1.25, 0.625, and 0.3125 mg/mL of HAp or Ge-HAp was added to the cells. The cultures were maintained for 1, 3, and 7 days, while the medium with fresh material was changed every other day. After 1/3/7 days, the supernatant was discarded, and 100 μL per well of MTT solution [3-(4,5-dimethylthiazolyl-2)-2,5 diphenyltetrazolium bromide, Sigma-Aldrich Inc., MA, USA] was added and incubated for 3 h at 37 °C. The precipitates were then dissolved in 100 μL of dimethyl sulfoxide (Sigma-Aldrich Inc., MA, USA) through shaking for 10 min at 37 °C. Optical density (OD) was measured using an enzyme-linked immunosorbent assay (ELISA) reader at 540 nm (RT- 2100c, Rayto, China). The cell viability (%) was calculated as

$$\frac{(OD_{sample} - OD_{blank})}{(OD_{control} - OD_{blank})} \times 100 \quad (1)$$

Osteoinductivity Assay. One day after cell seeding (1.5×10^5 cells/well in 24-well plate), 1 mL of osteogenic medium (StemMACS OsteoDiff Media, pH 7.4−7.8) with materials (1.25 mg/mL) was added per well. The cells were cultured for 7 days in the osteogenic medium supplemented with fresh HAp or Ge-HAp, which was replenished on the third day. The effect of Ge-HAp on the formation of mineralized nodules was examined by alizarin red S (ARS) staining. Cells were fixed with 4% neutrally buffered formalin for 30 min and stained with 2% ARS (Sigma-Aldrich). To quantify mineralization, ARS bound to cells was extracted by incubation with 250 μL of 1% hydrochloric acid in 70% ethanol for 20 min. The absorbance was measured at 450 nm on an ELISA microplate reader (RT-2100c, Rayto, China). The controls were the cells cultured only with osteogenic medium and HAp.

The effect of Ge-HAp on the expression level of osteodifferentiation markers (RUNX2, ALP, and OCN) was evaluated by RT-qPCR. Briefly, after osteoinduction of DPSCs for 7 days, total RNA was isolated from the cells using TRIzol Reagent (Invitrogen, Thermo Fisher Scientific, Waltham, Massachusetts, USA). The cDNA was prepared using Revert Aid First Strand cDNA Synthesis kit (Thermo Fisher Scientific) following manufacturer's instructions. RT-qPCR analysis was performed on a Line Gene-K Fluorescence Real-time PCR Detection System (Bioer, China) with Maxima SYBR Green/ROX qPCR Master Mix (Thermo Fisher Scientific). The sequences of human specific primers are presented in Table 1. The expression of GAPDH was used for normalization. The ΔΔCt method was used for the relative quantification of gene expression.[34]

Table 1. Primers with Corresponding Sequences Used in the Study

target		sense and antisense sequences 5′ to 3′
RUNX2	reverse	GTC TCG GTG GCT GGT AGT GA
	forward	ACA AAC AAC CAC AGA ACC ACA AGT
ALP	reverse	ATG GCA GTG AAG GGC TTC TT
	forward	CCA CGT CTT CAC ATT TGG TG
OCN	reverse	TCA GCC AAC TCG TCA CAG TC
	forward	GTG CAG AGT CCA GCA AAG GT
GAPDH	reverse	CCC TGT TGC TGT AGC CAA ATT CGT
	forward	TCA TGA CCA CAG TCC ATG CCA TCA

Fibroblastic Colony Forming Unit Assay. DPSCs (200 cells per well) were plated in six-well plates. Plates were incubated at 37 °C with 5% CO_2 after being seeded. At day 7 of the treatment with 1.25 mg/mL of Ge-HAp, cells were fixed with 4% paraformaldehyde for 15 min and stained for 30 min at the room temperature with 1.5% Crystal Violet. Microscopically and macroscopically, colonies that had been stained were counted. A group comprising more than 50 cells was considered as one colony. The formula for calculating the colony forming unit efficiency (%) was

$$\frac{\text{mean number of colonies}}{\text{total number of cells seeded}} \times 100 \quad (2)$$

Antibacterial Assay. Methicillin-resistant *S. aureus* (MRSA USA-300 strain; ATCC BAA-1680) and *E. coli* (Migula) Castellani and Chalmers (*E. coli*, ATCC 25922) obtained from the American Type Culture Collection (ATCC) were grown in tryptic soy broth (TSB) overnight. 1 mL aliquot (1 mL) was centrifuged at 6000 rpm for 2 min to pellet cells. The supernatant was discarded, and the pellet resuspended in 1 mL TSB. Dilutions of the bacteria (either MRSA or *E. coli*) in the broth were made to achieve an absorbance of 0.08−0.1 at 600 nm, which corresponds to a concentration of approximately 1×10^8 CFU/mL. This concentration was then serially diluted to 1×10^6 CFU/mL and used for the experiment. HAp and Ge-HAp were separately added to the bacteria, giving a final concentration of 60 mg/400 μL (150 mg/mL). One set of the supplemented and nonsupplemented bacterial cultures was incubated at 37 °C for 2 h, plated on tryptic soy agar (TSA) (2 control nonsupplemented plates, 2 HAp supplemented plates, and 2 Ge-HAp supplemented plates), and then incubated at 37 °C overnight. Another set of non-supplemented and supplemented bacterial cultures was incubated at 37 °C for 24 h, after which the culture dishes were plated on TSA (2 control nonsupplemented plates, 2 HAp supplemented plates, and 2

https://doi.org/10.1021/acsanm.3c05974
ACS Appl. Nano Mater. XXXX, XXX, XXX−XXX

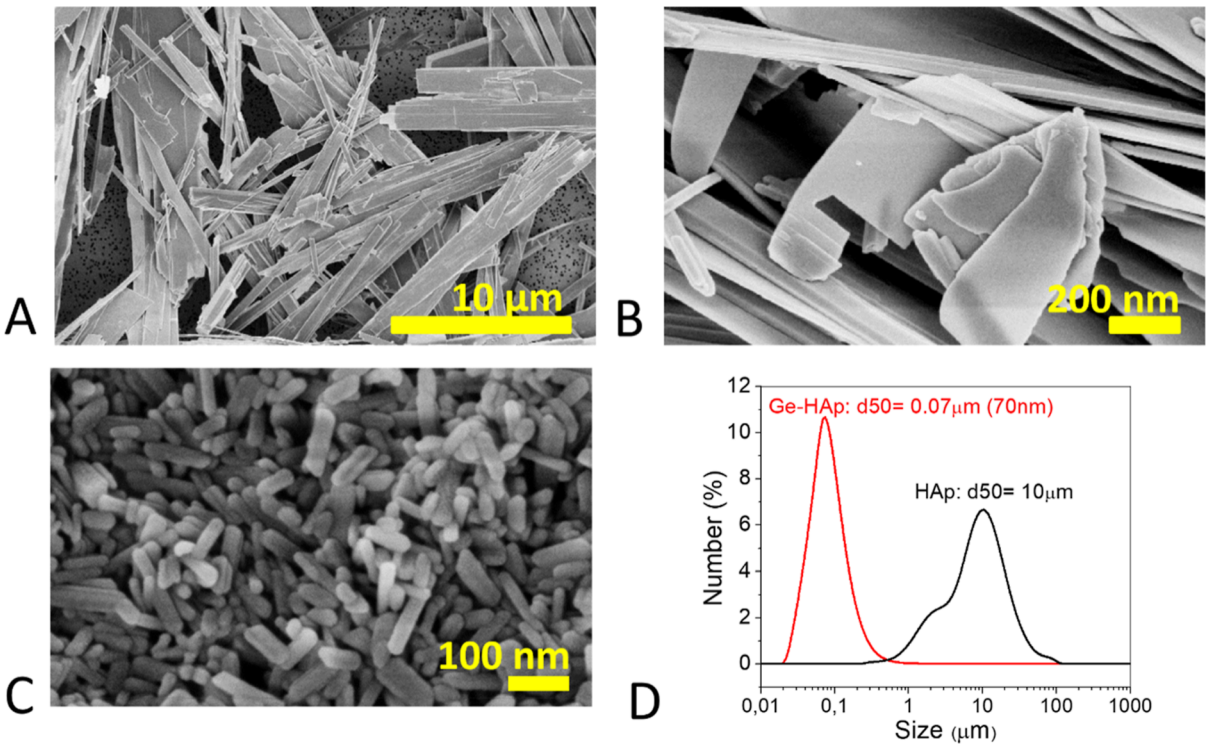

Figure 1. SEM images of (A,B) HAp and (C) Ge-HAp, along with (D) their distinct particle size distributions.

Ge-HAp supplemented plates) and then incubated at 37 °C overnight. Colonies were enumerated, digital images were obtained, and data were graphed to determine if there were any significant differences between the control and treated cultures. The antimicrobial dilutions used in this study were obtained from our published antimicrobial protocol.[35]

Antimycotic Assay. The reference strain of *C. albicans*, ATCC 10231 (Microbiologics KWIK-STIK, Manassas, VA, USA), was used. First, *C. albicans* was activated under aerobic conditions at 37 °C for 24 h using Sabouraud agar and Sabouraud dextrose broth (HiMedia, Mumbai, India). After the activation, McFarland 0.5 (approximately 10^6 yeast cells per ml) yeast suspension was prepared in sterile PBS. This suspension was diluted with the Sabouraud dextrose broth to a final concentration of 10^4 CFUs/mL and used for antimicrobial testing. Antimicrobial testing was conducted in a 96-well plate, using the following three groups: (1) negative control; (2) HAp group; and (3) Ge-HAp group. The negative control consisted of 100 μL of freshly prepared sterile Sabouraud dextrose broth and 100 μL of the yeast suspension (10^4 CFUs/mL). The HAp group consisted of 100 μL of nanoparticulate HAp suspension in Sabouraud dextrose broth (20 mg/mL) and 100 μL of yeast suspension (10^4 CFUs/mL). Each well in the Ge-HAp group consisted of 100 μL of Ge-HAp suspension in Sabouraud dextrose broth (20 mg/mL) and 100 μL of the yeast suspension (10^4 CFUs/mL). The experiment for each group was conducted in quintuplicate. The plate with the suspensions was incubated overnight under aerobic conditions at 37 °C. After 24 h, the antimicrobial effect was evaluated by seeding the suspensions using the Miles and Misra technique and eventually by comparing the number of CFUs/mL for each group. In brief, the overnight suspensions were diluted into eight 10-fold dilutions. 20 μL of each dilution was seeded on Sabouraud agar and incubated for 24 h at 37 °C under aerobic conditions. The number of CFUs/mL was calculated using the following formula:

$$\text{CFUs/mL} = \text{no. of colonies for a dilution} \times 50 \times \text{dilution factor} \quad (3)$$

The antimicrobial effect of HAp and Ge-HAp was determined by comparing CFUs/mL of these groups to CFUs/mL of the negative control.

Statistical Analysis. The software package GraphPad Prism ver. Nine was used for the analyses (GraphPad Software, Inc.). After examination of the distribution normality by the Kolmogorov–Smirnov normality test, ordinary one-way analysis of variance (ANOVA) and post hoc Tukey's multiple comparisons test with a single pooled variance were performed. The values are presented as mean ± SD. Statistical significance was set at $P < 0.05$ and marked as $^*P < 0.05$, $^{**}P < 0.01$, $^{***}P < 0.001$, and $^{****}P < 0.0001$.

RESULTS

Scanning Electron Microscopy. Both types of HAp nanoparticles assessed in this study, that is, HAp and Ge-HAp, were prepared under identical conditions involving hydrothermal precipitation and aging at 150 °C for 8 h. These conditions led to the formation of microsized sheets for HAp (Figure 1A,B) and much finer and more isotropic particles for Ge-HAp (Figure 1B). Particle size distribution histograms illustrating this difference are presented in Figure 1D. The physicochemical reasons for this change in particle size and morphology following the incorporation of GeO_3^{2-} ions were elaborated extensively in our earlier work.[28] In this previous study, we also estimated the composition of Ge-HAp at $Ca_{10-x}(PO_4)_{5.62}(GeO_3)_{0.38}(OH)_{2-y}$, with the GeO_3^{2-} ions naturally accommodating themselves at the crystallographic sites occupied by phosphate groups. The given composition was determined by the experimental measurement of the concentration of germanium per weight of Ge-HAp, while the subscripts x and y denote the necessity for the formation of paired calcium and hydroxyl vacancies required for stoichiometric charge compensation due to the replacement of trivalent phosphates with divalent germanates.

FTIR Spectroscopy. FTIR spectra of HAp and Ge-HAp in the 4000–400 cm^{-1} wavenumber range are shown in Figure 2. The antisymmetric (ν_3) stretching mode of the phosphate tetrahedron dominates the spectra of both HAp and Ge-HAp

https://doi.org/10.1021/acsanm.3c05974
ACS Appl. Nano Mater. XXXX, XXX, XXX−XXX

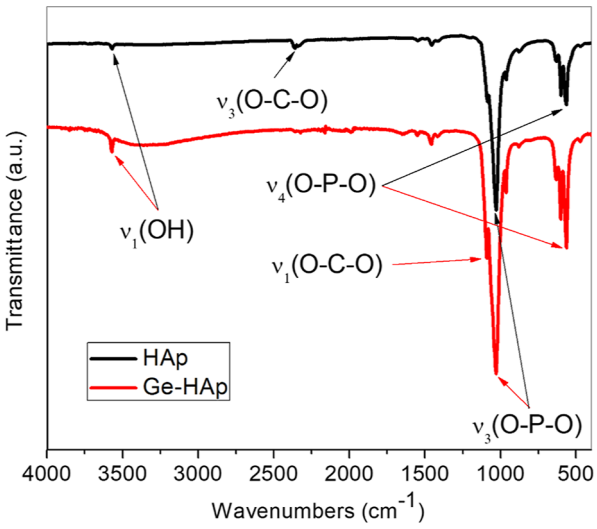

Figure 2. FTIR spectra of HAp and Ge-HAp in the 4000−400 cm^{-1} wavenumber range.

and the only difference between them is seen in the distribution of carbonate bands. Namely, while the symmetric (ν_1) stretching mode of the carbonate group appears to be more dominant in the spectrum of Ge-HAp, the corresponding antisymmetric (ν_3) vibration mode is more dominant in the spectrum of HAp. These subtle alterations are consequential to the structural disorder introduced to the material with the addition of Ge in the form of germanate ions. Namely, carbonate is the main inadvertent dopant in HAp due to its atmospheric origins and the competition between carbonates and germanate ions for the phosphate groups of HAp is likely to induce a redistribution of carbonates in Ge-HAp as compared to the order these groups assume in HAp, which becomes evidenced in FTIR spectra. Other notable bands originating from the vibrations of the hydroxyl and phosphate groups are denoted in Figure 2.

Nanoparticle Uptake. Upon the flow cytometric examination of cells treated with Ge-HAp, SSC, which indicates distinctions in the physical state of the cell, including those due to the uptake of particles, increased with increasing Ge-HAp concentration. The sole exception was the 1.25 mg/mL concentration, which demonstrated a greater uptake than the 2.5 mg/mL concentration (Figure 3). Interestingly, FSC, which is commonly used to compare the cellular size, did not reveal any significant changes in the cellular size upon uptake.

DPSC Viability. Neither of the HAp materials, be they Ge-free or doped with Ge, showed any considerable cytotoxicity in DPSCs, even at the highest dose (5 mg/mL) and incubation time (7 days) tested. This can be concluded from the fact that no sample groups except 5 mg/mL HAp exhibited a reduction in the cell viability below that of 70% (dotted line in Figure 4) relative to the negative control. Still, from the viability data shown in Figure 4, it is evident that two factors of the treatment are inversely proportional to cell viability, one of which is the particle dose, and the other one of which is the incubation time.

Interestingly, at the shortest incubation time of 1 day, the viability of cells exposed to fine doses of HAp exceeded the viability of the control cells. In contrast, for all of the particle concentrations, the viability of cells exposed to Ge-HAp was significantly lower than that of cells exposed to HAp. Meanwhile, only the viability of cells treated with the highest concentration of Ge-HAp was statistically significantly ($P < 0.05$) lower than that of the control (Figure 4A). Furthermore, the viability of cells consistently dropped as the particle dose increased, with trends applicable to both HAp and Ge-HAp.

After 3 days, some of these trends remained, and some of them changed (Figure 4B). For one, the viability of cells exposed to Ge-HAp continued to be lower than that of cells exposed to HAp and this trend applied to every particle

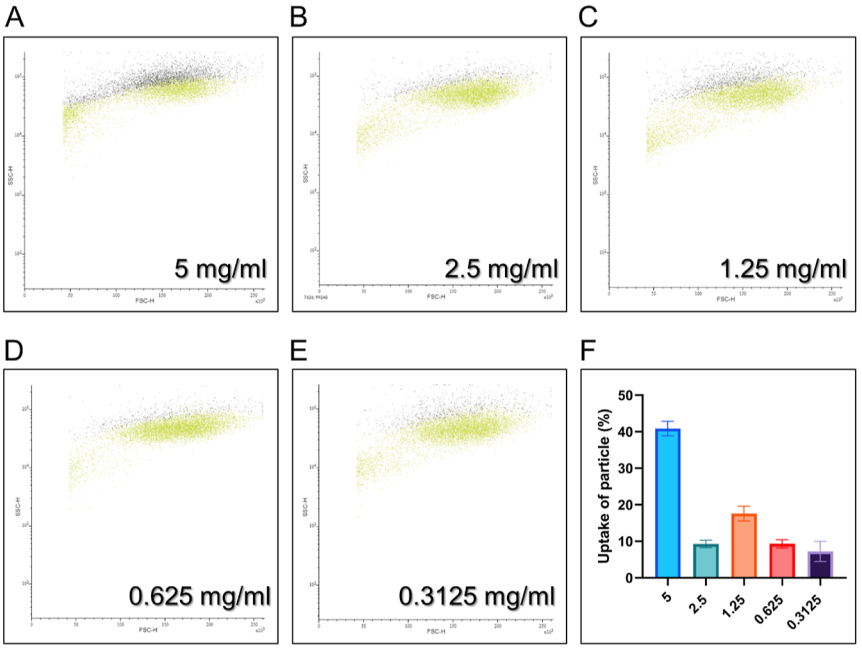

Figure 3. Cytograms (A−E) of FSC (linear scale) and SSC (log scale), demonstrating that SSC increases in Ge-HAp-treated cells relative to untreated cells (green dots). The highest percentage of nanoparticle uptake (F) was observed at the maximum concentration (5 mg/mL). Data bars denote averages ($n = 6$) and error bars the standard deviation.

https://doi.org/10.1021/acsanm.3c05974
ACS Appl. Nano Mater. XXXX, XXX, XXX−XXX

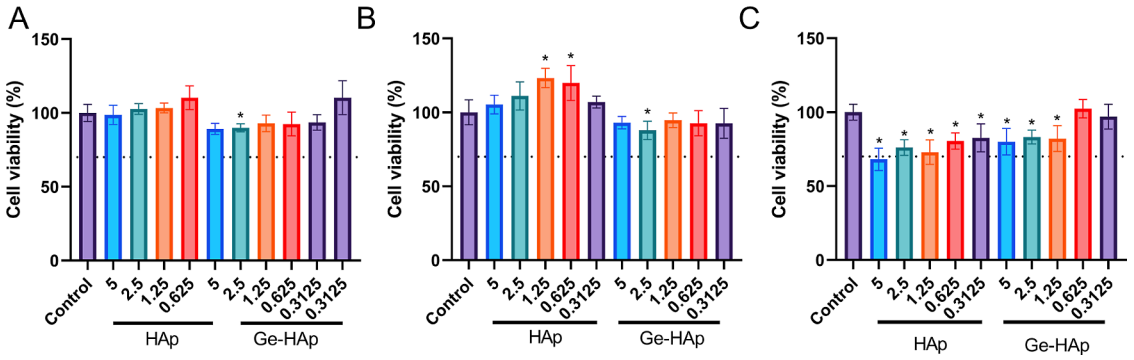

Figure 4. Cell viability after (A) 1, (B) 3, and (C) 7 days of treatment with HAp or Ge-HAp at different concentrations (mg/mL on x-axis). Data bars denote averages (n = 18) and error bars the standard deviation. *P < 0.05 for the sample vs the control.

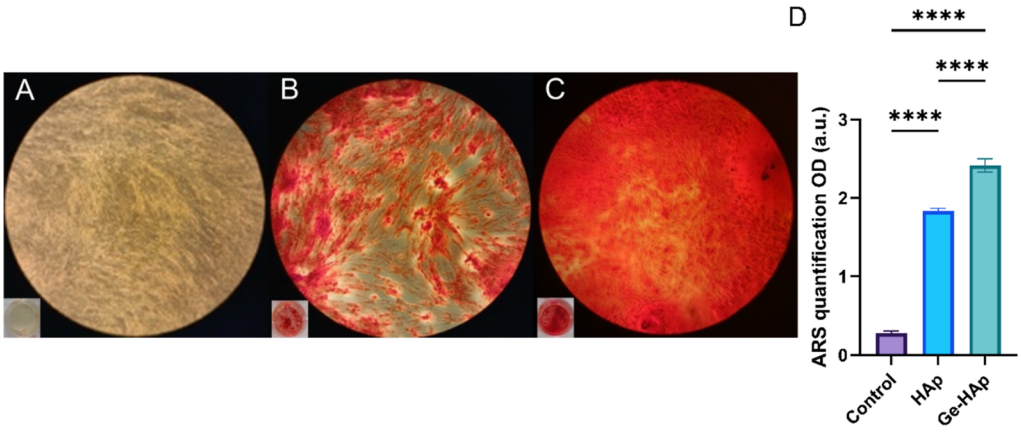

Figure 5. Inverted light microscopic and macroscopic representative images of alizarin red staining. Original magnification 40×. (A) Control (without material), (B) cells treated with HAp, (C) cells treated with Ge-HAp, and (D) the mean absorbance of ARS. Data bars denote averages (n = 18) and error bars the standard deviation. ****P < 0.0001.

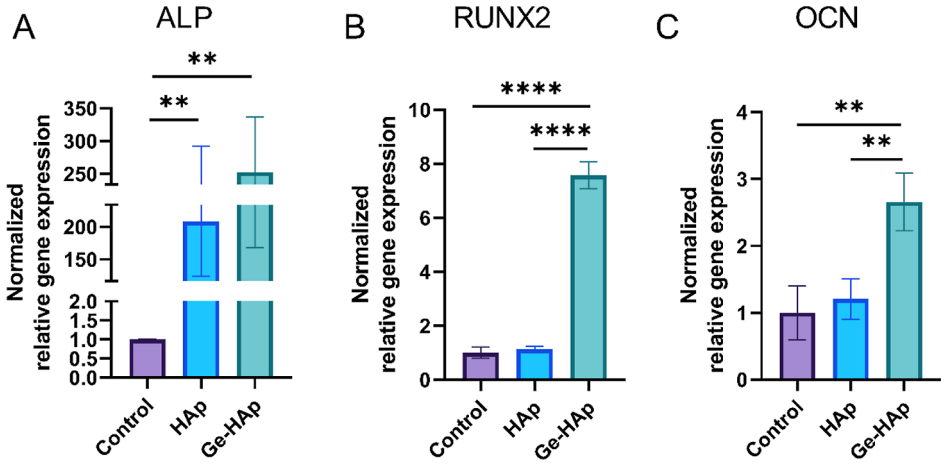

Figure 6. Quantitative analysis of relative mRNA expression for osteogenesis related genes (A) ALP, (B) RUNX2 and (C) OCN in control cells, cells treated with HAp, and cells treated with Ge-HAp. Data bars denote averages (n = 18) and error bars the standard deviation. **P < 0.01 and ****P < 0.0001.

concentration. However, for both HAp and Ge-HAp, the viability increased with the dose up to 1.25 mg/mL, and only then did it begin to drop. Also, interestingly, the viability of cells grown at the two lowest doses of HAp, i.e., 0.3125 and 0.625 mg/mL, was statistically significantly higher than that of the control, speaking to the ability of HAp to boost the viability of cells. A similar trend was not detected among cells treated with Ge-HAp, for which the viability was lower than that of the control at all the particle concentrations. The viability experiments enabled us to determine the particle concentration of 1.25 mg/mL for further experiments. This concentration was derived based on the observed trends in cell viability across different particle concentrations and incubation times, as well as the balance between promoting cell viability and avoiding cytotoxic effects.

https://doi.org/10.1021/acsanm.3c05974
ACS Appl. Nano Mater. XXXX, XXX, XXX−XXX

As the duration of the incubation of the cells with the particles was extended up to 7 days, the trends significantly changed (Figure 4C). First, the viability of cells exposed to each HAp particle concentration was statistically significantly lower than that of the control at the end of this incubation. Also, the viability consistently dropped with the particle concentration. Interestingly, for Ge-HAp, the statistically significant reduction of viability was observed only at particle concentrations higher than or equal to 1.25 mg/mL, but not for the lower concentrations. In fact, the viabilities of cells exposed to Ge-HAp for 7 days at concentrations of 0.3125 and 0.625 mg/mL were statistically significantly higher than those of any other sample groups.

Alizarin Red Staining. To study the effect of Ge-HAp on mineralization in DPSCs in comparison to the effect of HAp, alizarin red staining was performed, and significant differences in the quantity of mineralization were observed among the groups (Figure 5A–C). One-way ANOVA revealed these differences to be significant ($P < 0.0001$) (Figure 5D). The Ge-HAp group had a significantly increased amount of mineralized nodule formation compared to the control cells treated only with the osteogenic medium and compared to the cells treated with Ge-free HAp. Evidently, HAp acts as a mineralization promoter, but this role becomes significantly more pronounced with the addition of Ge to it.

Influence of Ge-HAp on Bone-Related Gene Expressions of DPSCs. After 7 days of osteogenic induction with Ge-HAp, osteogenesis-related genes of DPSCs, including ALP, RUNX2, and OCN, were shown to be significantly upregulated compared to both the control cells and cells exposed to Ge-free HAp (Figure 6). The most significant effect of Ge addition to HAp was observed in RUNX2 expression, with HAp producing a minimal difference with respect to the control and the addition of Ge to HAp leading to a 6.6-fold increase in expression (Figure 6B). Next, there was a nonsignificant increase in OCN expression with HAp supplementation and a significant 2.2-fold increase when Ge-HAp was added (Figure 6C). Furthermore, both HAp and Ge-HAp elevated gene expression of ALP, which was more pronounced for Ge-HAp than it was for HAp, even though no statistically significant difference was found between HAp and Ge-HAp (Figure 6A).

Fibroblastic Colony Forming Unit Assay. MSCs were formerly known as fibroblastoid colony forming cells because of their propensity to attach to tissue culture plastic and develop clonogenic cell clusters when plated at low densities. The efficiency with which they form colonies continues to be a key indicator of the cell quality.[36] Thus, more mature and differentiated cells should give fewer clonogenic cell clusters. As shown in Figure 7, during the treatment with Ge-HAp, DPSCs formed significantly less colonies compared to the control ($P < 0.05$). Both HAp and Ge-HAp reduced the ability of DPSCs to form colonies, but this effect was, evidently, more pronounced for Ge-HAp than it was for HAp.

The Antibacterial Effect. Colony enumeration after 2 h of incubation with HAp or Ge-HAp supplemented MRSA cultures on agar plates revealed significant differences ($p = 0.0199$) in colony count between the control and the treated groups. Ge-HAp and HAp supplemented MRSA showed 40 and 60% decreases in colony count, respectively. Likewise, the supplemented MRSA cultures that were incubated for 24 h before plating on agar also revealed an observable difference in colony counts between HAp and Ge-HAp supplemented

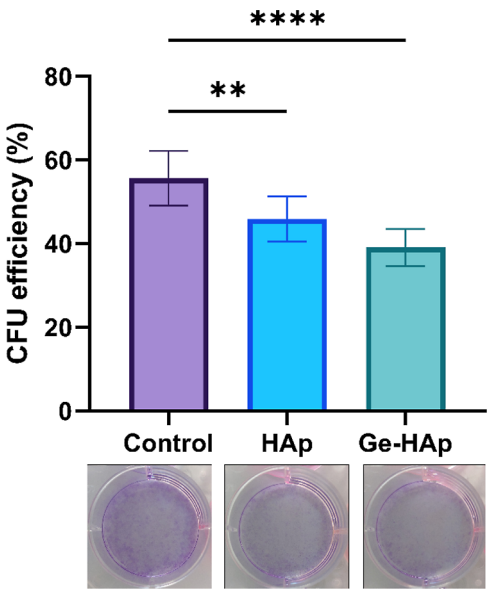

Figure 7. Number of colonies formed after the 7 day-treatment with HAp or Ge-HAp relative to the control. Data bars denote averages ($n = 18$) and error bars the standard deviation. $^{**}P < 0.01$ and $^{****}P < 0.0001$.

cultures when compared to nonsupplemented controls (Figure 8A,B). Due to overgrowth, the colonies could not be enumerated; however, a qualitative difference in colony layout could be seen (Figure 8A, bottom panel).

Supplementation of *E. coli* cultures with HAp or Ge-HAp showed no difference in the colony enumeration between the supplemented and control groups. In fact, there was a slight nonsignificant increase in colony count of *E. coli* that was supplemented with HAp (Figure 9A,B). Data after 24 h of incubation of *E. coli* with both HAp and Ge-HAp followed the same trend with colony enumeration, which was difficult to obtain due to overgrowth of the bacteria (Figure 9A, lower panel).

Antifungal Effect. The results of the antifungal analysis showed a significant decrease in CFU/mL values of *C. albicans* in the Ge-HAp group compared to HAp and control (untreated) groups, indicating a robust antimicrobial effect of the former material (Figure 10). It is notable that undoped HAp showed a considerable antimicrobial effect, although the observed difference was at the borderline of statistical significance ($p = 0.0657$), suggesting a lower impact on fungal cell proliferation than that accomplished by its Ge-doped counterpart.

DISCUSSION

The current study employed one of the most accessible sources of stem cells in the oral cavity, namely, DPSCs, and used them to assess biocompatibility, the osteoinductive effect and antimicrobial properties of Ge-doped HAp. One main finding of this study refers to the high osteogenic induction of DPSCs in the presence of Ge-HAp. Directly supporting this finding, alizarin red staining experiments showed a greater extent of mineral deposition in cultures exposed to HAp doped with Ge than in any other sample groups. HAp evidently increased the mineral deposition in cell cultures, but judging based on the difference in the mineral deposition extent, the addition of Ge to HAp provided an even more intense osteogenic effect.

https://doi.org/10.1021/acsanm.3c05974
ACS Appl. Nano Mater. XXXX, XXX, XXX−XXX

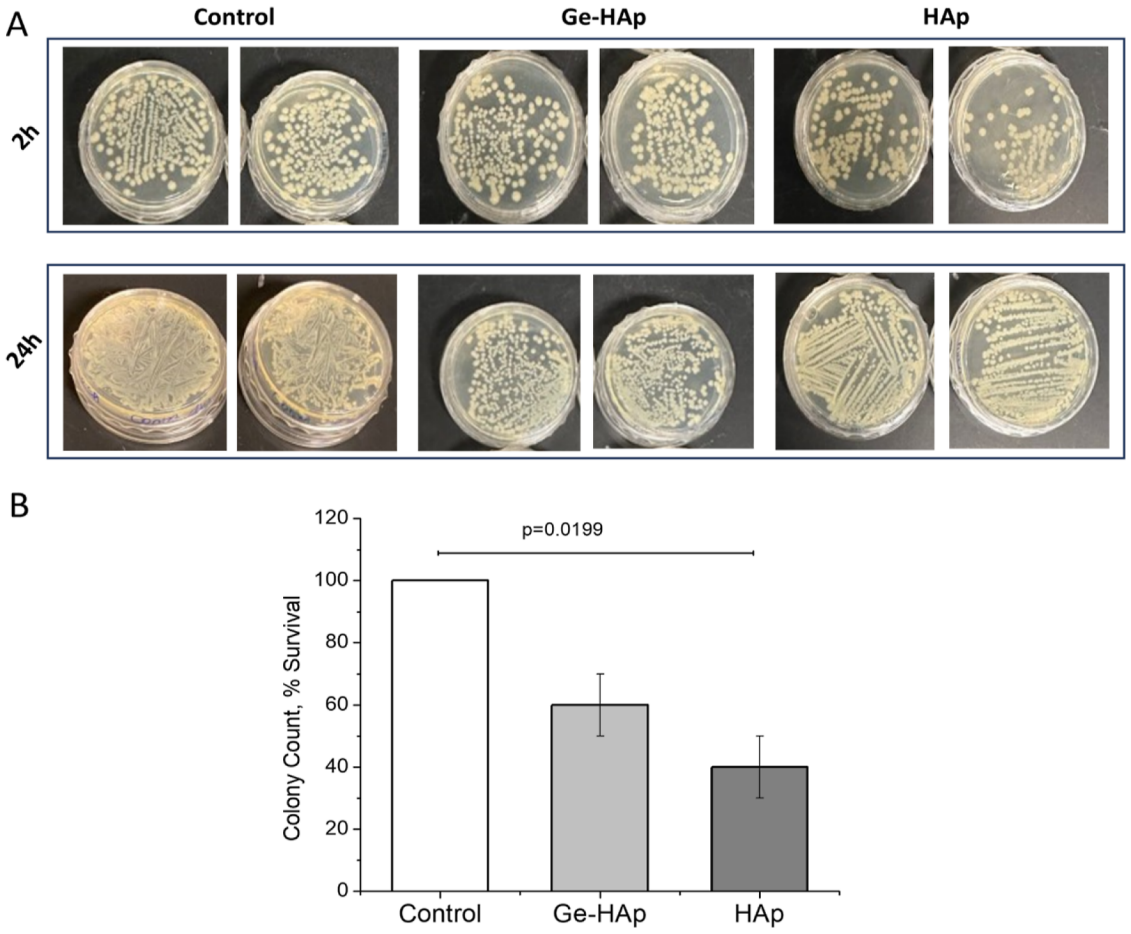

Figure 8. (A) Representative photographs of MRSA colonies after 2 and 24 h incubations of supplemented cultures, along with (B) the quantification. Data bars denote averages (n = 3) and error bars the standard deviation.

In addition, the osteogenic differentiation of DPSCs was assessed in cells exposed to the osteogenic medium alone as well as in cells exposed to HAp or Ge-HAp supplemented medium. The osteoinductive effect was confirmed in three different osteogenesis-related genes: ALP, RUNX2, and OCN. ALP is a ubiquitous enzyme and a well-known marker indicative of early mineralization, given that ALP secretion occurs during osteoblast maturation and bone matrix mineralization.[37] RUNX2 is a key transcription factor that is linked to bone formation and acts as the first and most specific signal mediator, activating and regulating osteogenic differentiation. It also plays an important role in the differentiation of the preosteoblastic cells to mature osteoblasts.[38] Finally, OCN has important roles in maturation of mineralized tissues and regulation of the osteogenic differentiation of MSCs, where it facilitates mineral deposition, regulates osteoblast and osteoclast function, and influences mineral and energy metabolism.[39] In contrast to ALP and RUNX2, OCN is exclusively generated by completely developed osteoblasts and is, thus, a mature osteoblast marker.[40] Various extracellular ligands such as bone morphogenetic proteins (BMPs), Wnt and fibroblast growth factors control the osteogenic differentiation of the different multipotent MSCs.[41] These ligands direct the three main stages of the osteogenic differentiation, which are associated with the expression of genes such as BMP-2, RUNX2, OCN, and osteonectin.[42] Previously, HAp nanoparticles were discovered to have a favorable impact on osteogenesis.[43−45] For example, HAp nanoparticles with a diameter of around 20 nm increased the expression of type I collagen, OCN, and OPN in rabbit MSCs.[43] In the current study, doping HAp with Ge significantly upregulated each of the three osteogenesis-related genes assessed relative to both the control cells and cells treated with Ge-free HAp. A more augmentative effect was observed for RUNX2 than for OCP, suggesting that although Ge affects both the differentiation and maturation stages of the osteogenic process, its effect is more decisive early on, in the differentiation stage. This may explain the more reductive effect of Ge-HAp on cellular proliferation at early incubation times as opposed to the longer ones, considering that proliferation and differentiation are mutually exclusive.[46−48] ALP is the most ambiguous marker of the three genes analyzed, and both HAp and Ge-HAp produced an enormous augmentative effect on its expression, although the effect of Ge-HAp was evidently more intense than that of HAp. In short, supplementation of HAp with Ge can be used to promote early differentiation of stem cells into osteoblastic lineages to a great effect.

Cellular absorption of nanoparticles is an important factor in assessing nanotoxicity. Flow cytometry has the ability to analyze thousands of cells in a matter of seconds. In these analyses, the side-scatter light signal is used as a measure of the nanoparticle uptake.[49] In this study, the highest concentration of Ge-HAp resulted in the highest uptake of the nanoparticles by DPSCs relative to the total nanoparticle dose. At this highest nanoparticle concentration, namely, around 40% of the particles ended up being taken up by the cells. However, a

https://doi.org/10.1021/acsanm.3c05974
ACS Appl. Nano Mater. XXXX, XXX, XXX−XXX

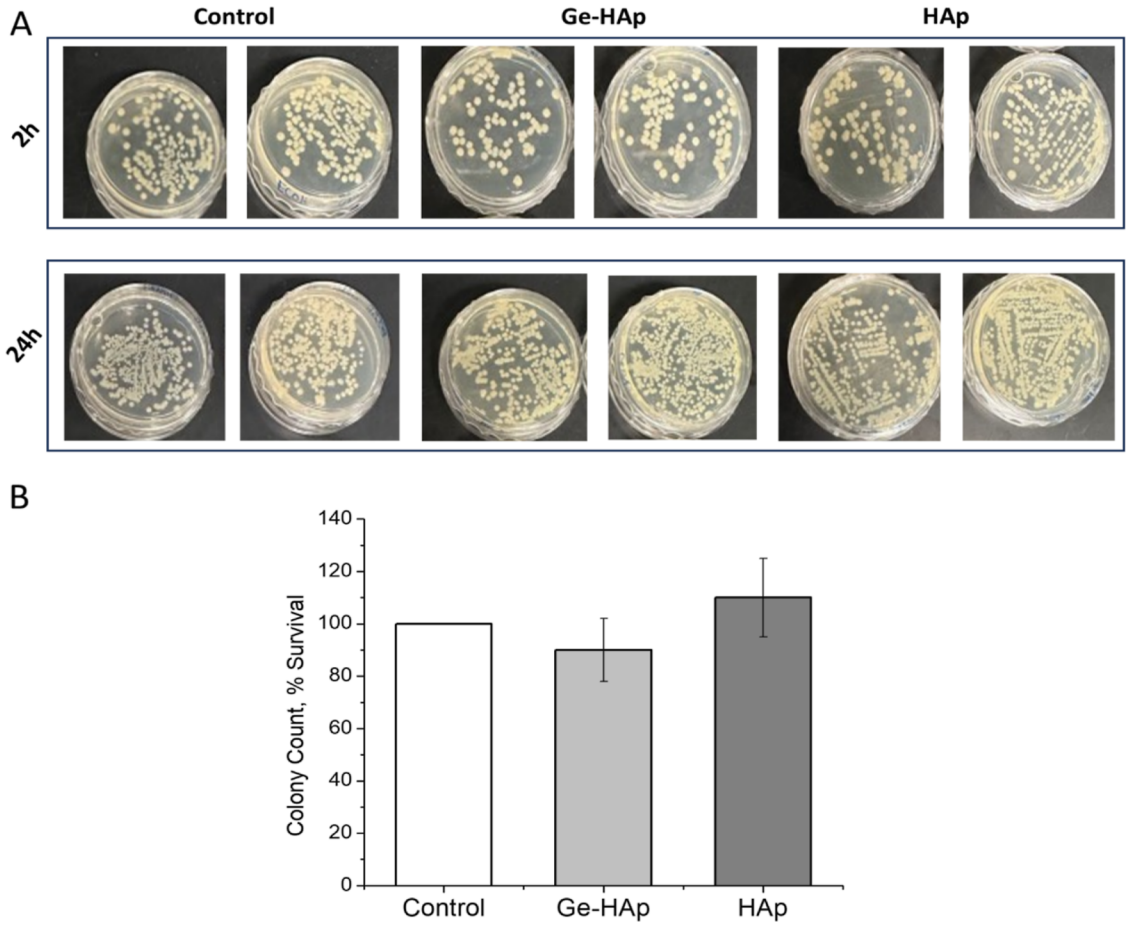

Figure 9. (A) Representative photographs of *E. coli* colonies after 2 and 24 h incubations of supplemented cultures, along with (B) quantification. Data bars denote averages (n = 3) and error bars the standard deviation.

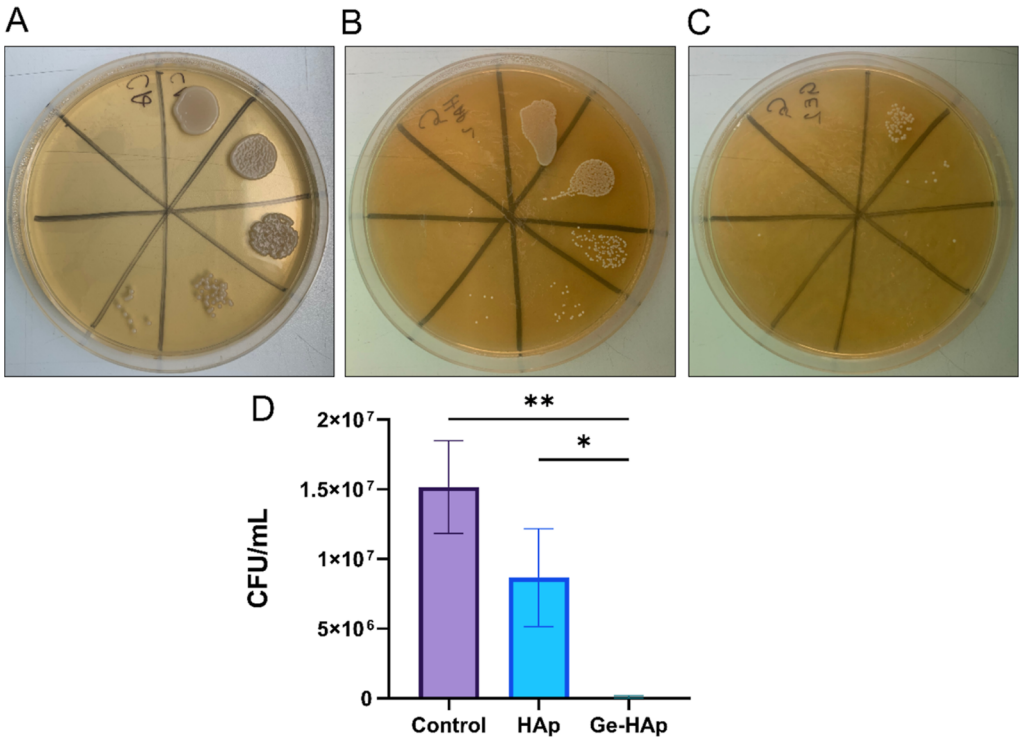

Figure 10. Antimycotic effect of HAp and Ge-HAp. Representative photographs of *C. albicans* colonies in (A) control (untreated), (B) HAp, and (C) Ge-HAp groups; (D) quantification. Data bars denote averages (n = 6) and error bars the standard deviation. *P < 0.05 and **P < 0.01.

https://doi.org/10.1021/acsanm.3c05974
ACS Appl. Nano Mater. XXXX, XXX, XXX−XXX

dose-dependent trend was not observed. It seemed that the concentration of 1.25 mg/mL was the most favorable for the DPSCs apart from the highest. The surface charge of nanoparticulate HAp is known to affect their absorption by the cells as well as other aspects of their biological response.[50] In a study by Chen et al., for example, MC3T3-E1 cells took up positively charged nanoparticulate HAp more than other nanoparticles of comparable size.[50] This was due to the electrostatic attraction between positively charged HAp and the negative charge of the cell membrane. However, the particle concentration in the medium should not affect the surface charge to such a degree as to justify the rather dramatic increase in the uptake percentage with the particle concentration. A more likely mechanism may be the increased sedimentation of the nanoparticles at higher concentrations. In planar cell culture, such as that utilized here, the uptake is favored when nanoparticles are unstable in suspension and sediment, an effect that becomes more pronounced for many dispersions as the concentration of the dispersed phase is increased.[51] The competing effect, however, comes in the form of agglomeration of nanoparticles, which adversely affects the uptake when the size of the agglomerates exceeds a specific threshold.

Also, in the current study, cytotoxicity of Ge-HAp was measured by looking at the viability of DPSCs in the presence of different doses of Ge-HAp or HAp with respect to the negative controls after different incubation periods of 1, 3 and 7 days. Moderately cytotoxic effect, as indicated by the cell viability of 68%, was observed only at the highest concentration of HAp (5 mg/mL). Many earlier studies have documented the dose-dependent cytotoxicity of HAp nanoparticles in various cell types, where they trigger necrosis or apoptosis.[52−56] The HAp nanoparticle load has demonstrated a high degree of association with cell death.[53,55] In these prior studies, HAp nanoparticles were metabolized in cell lysosomes, which raised intracellular Ca^{2+} concentrations and led to lysosomal rupture and cell necrosis.[57] Furthermore, the expected aggregation and subsequent sedimentation of HAp nanoparticles at very high concentrations may induce mechanical damage to the cells, resulting in cytotoxicity.[52]

The greater degree of dose-dependent cytotoxicity exhibited by Ge-HAp as compared to HAp at lower incubation times and the lower degree of it present at longer incubation times could be attributed to either the compositional or structural effects. As for the compositional effects, they are solely related to the administration of Ge in the form of germanate ions, which may affect cellular metabolism and gene expression pathways in the direction of reduced viability in the early phase of incubation. This reduced viability, however, gets compensated by accelerated osteogenic differentiation evident from the gene expression analyses. Further, the viability reduction effect gets reversed at later stages of incubation, as the result of which the viability gets restored. As for the structural effects, they stem from changes in the physical properties of HAp nanoparticles resulting from the accommodation of Ge. A most notable of such effects is the change in particle size and morphology, as elongated HAp sheets have been shown to transition to finer rods with the introduction of Ge. Furthermore, in our previous study,[28] we demonstrated an increased crystallographic disorder resulting from this accommodation. Here, more entropic nanoparticles, exhibiting lower crystallinity and higher solubility, can be imagined to produce a different effect on viability and osteoinductivity in stem cells compared to their more crystalline and less soluble counterparts. The pH of the medium in which the cell culture with the nanoparticles was performed was mildly alkaline (7.4−7.8 for the osteogenic medium and 6.9−7.3 for DMEM), and under those conditions, the dissolution of either HAp or Ge-HAp should be negligible; however, once accommodated inside the acidic lysosomal compartments, the dissolution becomes considerable and supposedly greater for the more structurally disordered and morphologically finer Ge-HAp than for HAp.

The rise in the resistance of microorganisms to commonly available antibiotics has necessitated the search for alternative antimicrobial compounds. Two of the compounds synthesized and tested in this study have been the nanoparticles of HAp and Ge-HAp. One of the objectives was to characterize the antimicrobial effect of these compounds on two bacteria of medical importance: Gram-positive MRSA and Gram-negative *E. coli*. The results indicate that HAp and Ge-HAp have the potential to significantly inactivate and suppress the growth of MRSA. However, when these nanoparticles were tested against *E. coli*, the outcome was different with no antimicrobial effect recorded. These data revealed that the potential for HAp and Ge-HAp to inactivate microorganisms vary.

Previously, Wu et al.[58] had shown that amorphous calcium phosphate (ACP) and HAp nanoparticles inactivated both Gram-positive and Gram-negative bacteria including *S. aureus*, *Staphylococcus epidermis*, *Enterococcus faecalis*, *E. coli*, *Pseudomonas aeruginosa*, and their multidrug-resistant analogues, albeit with a different Gram-positive versus Gram-negative selectivity. Thus, even though the antimicrobial activities of ACP and HAp were similar against Gram-negative microorganisms, ACP proved to be more effective against the Gram-positive ones, for which HAp was less effective in comparison.[58] Still, a definite antibacterial activity of HAp was evidenced in these former studies, which demonstrated not only the selective antibacterial performance of HAp nanoparticles against selected bacterial types and laboratory or clinical strains, but also the ability of these nanoparticles to hijack the efflux pump system and inhibit the bacterial growth through intracellular localization.[58−60]

The results obtained in this study are similar to the observed data in the Wu et al. study;[58] however, there is a difference in the inactivation of *E. coli*. Whereas the previous study showed some activity against *E. coli*, the present study seems to differ with no observed antimicrobial activity. Several factors play a role in the inactivation of bacteria by nanoparticles, including (i) the type of nanoparticles, (ii) the concentration of the nanoparticles, (iii) the bacterial strain, (iv) the mechanism of action of the nanoparticles, and (v) the specifics of the assay utilized. Hence, when evaluating the potential of these nanoparticles to inactivate various strains of bacteria, all these factors have to be taken into consideration. That nanoparticles of HAp or Ge-HAp did not exhibit a similar activity in this study as in the aforementioned prior one can be ascribed with the greatest degree of probability to their different physicochemical properties. Namely, while antibacterial HAp in the aforementioned prior study was synthesized using a wet chemical procedure that did not employ any elevated thermal treatment, HAp nanoparticles tested in this study were prepared under hydrothermal conditions, which favor larger and more structured particles, with a likely lower potential to translocate across biological barriers, invade the bacterial cells and disrupt their proliferative machinery. The data reported here, however, were derived on two bacterial

https://doi.org/10.1021/acsanm.3c05974
ACS Appl. Nano Mater. XXXX, XXX, XXX−XXX

strains alone in parallel planktonic and agar assays, which is not to discard the possibility that their effect against different strains and/or under different testing conditions can be more pronounced than that observed here. Nevertheless, the excellent safety profile and positive eukaryotic versus prokaryotic cell selectivity of these nanoparticles warrants further investigation. As such, future studies will attempt to optimize this protocol against MRSA and investigate the possible mechanisms of bacterial inactivation by these nanoparticles.

The antimicrobial activity of the nanoparticles was also assessed against *C. albicans* as the fungal species of choice. It was shown that at the ratio of the colony forming units to the nanoparticle weight in milligrams of 500, the population of the fungi gets completely obliterated by Ge-HAp, but not by HAp, even though both materials diminish this population by a considerable amount. Overall, the simultaneity of the antimicrobial activity and the osteoinductive potential of the nanoparticles is promising from the perspective of applicability in the dental and medical repair of hard tissues. However, optimization of Ge accommodation inside the crystal lattice of HAp and of physical properties of the nanoparticles is needed to further improve the exciting set of biological properties displayed by this material.

CONCLUSIONS

This study presents the first investigation of the biological properties of Ge-HAp. Cytotoxicity, the osteogenic differentiation propensity, the colony formation potential of DPSCs, the antibacterial effect against *E. coli* and MRSA, and the antifungal effect against *C. albicans* brought to contact with Ge-HAp were included among these properties and systematically compared against the same sets of properties exhibited by HAp and by appropriate experimental controls. The addition of Ge to HAp produced a lower cell viability than that induced by HAp after 24−72 h incubation periods, but the effect was reversed after a week-long incubation, when low doses of Ge-HAp produced significantly higher cell viabilities than those produced by HAp. Both HAp and Ge-HAp induced mineral formation in the cell culture, but the effect was considerably more pronounced for Ge-HAp. Likewise, Ge-HAp upregulated the expression of all three osteogenic markers analyzed relative to those of both control cells and cells exposed to Ge-free HAp. A more augmentative effect was observed for RUNX2 than for OCN, suggesting that although Ge stimulates both the differentiation and maturation stages of the osteogenic process, its effect may be more pronounced in the early differentiation stage. The colony formation capacity of stem cells was impaired by HAp and even more so by Ge-HAp, which was expected considering that more mature and differentiated cells are less prone to form clonogenic colonies. The nanoparticles were well taken up by the cells but without producing any morphological changes detectable by flow cytometry. The antimicrobial effect of the nanoparticles was greatly dependent on the microorganisms tested. Whereas the antimicrobial activity was absent against *E. coli*, it was evident against MRSA and *C. albicans*. However, while the antibacterial activity against MRSA was weakened by the addition of Ge to HAp, the antimycotic activity against *C. albicans* was intensified with the addition of Ge, completely obliterating the microorganisms at the ratio of the colony forming units to the nanoparticle weight in milligrams of 500.

Research presented here demonstrates that Ge-doped HAp nanoparticles could have significant potential in the field of regenerative medicine due to their high biocompatibility and osteoinductivity. Given that a single concentration of Ge oxyanions produced an effect on the physical and biological properties of HAp as intense as those evidenced in this study, it can be expected that inspection of broader ranges of concentrations of Ge in Ge-HAp might lead to the observation of additional interesting effects. Besides, further optimization of physical properties and Ge accommodation inside the crystal lattice of HAp is needed to boost the antibacterial effect of these nanoparticles and capitalize on the heavily sought duality of osteogenic and antimicrobial properties in a single material. Findings reported here may be used as the basis for prolific further exploration of HAp and Ge-HAp in nanomedicine and tissue engineering.

AUTHOR INFORMATION

Corresponding Author

Vuk Uskoković − *TardigradeNano, Irvine, California 92604, United States; Department of Mechanical Engineering, San Diego State University, San Diego, California 92182, United States;* orcid.org/0000-0003-3256-1606; Email: vuk.uskokovic@tardigradenano.com

Authors

Miloš M. Lazarević − *School of Dental Medicine, University of Belgrade, 11000 Belgrade, Serbia;* orcid.org/0000-0003-1330-5332

Nenad L. Ignjatović − *Institute of Technical Sciences of the Serbian Academy of Science and Arts, 11000 Belgrade, Serbia;* orcid.org/0000-0002-5749-094X

Qene Mahlet − *Department of Chemistry and Biochemistry, San Diego State University, San Diego, California 92182, United States*

Violet V. Bumah − *Department of Chemistry and Biochemistry, San Diego State University, San Diego, California 92182, United States; Department of Chemistry and Physics, University of Tennessee at Martin, Martin, Tennessee 38237, United States*

Milena Radunović − *School of Dental Medicine, University of Belgrade, 11000 Belgrade, Serbia*

Jelena Milašin − *School of Dental Medicine, University of Belgrade, 11000 Belgrade, Serbia*

Dragan P. Uskoković − *Institute of Technical Sciences of the Serbian Academy of Science and Arts, 11000 Belgrade, Serbia*

Complete contact information is available at: https://pubs.acs.org/10.1021/acsanm.3c05974

Author Contributions

The manuscript was written through contributions of all authors. All authors have given approval to the final version of the manuscript.

Notes

The authors declare no competing financial interest.

ACKNOWLEDGMENTS

This research was funded by the Science Fund of the Republic of Serbia, #grant no. 7750038, Oral cancer—new approaches in prevention, control, and postoperative regeneration—an in vitro study—ORCA−PCR; the Ministry of Science, Technological Development and Innovation of the Republic of Serbia

https://doi.org/10.1021/acsanm.3c05974
ACS Appl. Nano Mater. XXXX, XXX, XXX−XXX

on the research programs: grant no. 451-03-47/2023-01/200129 (University of Belgrade, School of Dental Medicine) and grant no. 451-03-66/2024-03/200175 (Institute of Technical Sciences of SASA). The authors also acknowledge the help of Dr. Srečo Škapin (Jožef Stefan Institute, Ljubljana, Slovenia) for the SEM analysis and Prof. Chukuka Enwemeka's generous provision of lab space and resources at San Diego State University for performing the antibacterial assays.

■ ABBREVIATIONS

HAp, hydroxyapatite; Ge-HAp, germanium-doped hydroxyapatite; MRSA, methicillin-resistant *Staphylococcus aureus*; MSCs, mesenchymal stem cells; DPSCs, dental pulp stem cells; OCN, osteocalcin; RUNX2, runt-related transcription factor 2; ALP, alkaline phosphatase; FE-SEM, field-emission scanning electron microscopy; DMEM, Dulbecco's Modified Eagle Medium; FBS, fetal bovine serum; FSC, forward light scatter; SSC, side light scatter; DMSO, dimethyl sulfoxide; OD, optical density; ARS, alizarin red S; TSA, tryptic soy agar; ATCC, American Type Culture Collection; ACP, amorphous calcium phosphate; MDR, multidrug-resistant

■ REFERENCES

(1) Yu, L.; Zeng, L.; Zhang, Z.; Zhu, G.; Xu, Z.; Xia, J.; Weng, J.; Li, J.; Pathak, J. L. Cannabidiol Rescues TNF-α-Inhibited Proliferation, Migration, and Osteogenic/Odontogenic Differentiation of Dental Pulp Stem Cells. *Biomolecules* **2023**, *13* (1), 118.

(2) De Bonis, A.; Uskoković, V.; Barbaro, K.; Fadeeva, I.; Curcio, M.; Imperatori, L.; Teghil, R.; Rau, J. V. Pulsed Laser Deposition Temperature Effects on Strontium-Substituted Hydroxyapatite Thin Films for Biomedical Implants. *Cell Biol. Toxicol.* **2020**, *36* (6), 537−551.

(3) Fadeeva, I. V.; Lazoryak, B. I.; Davidova, G. A.; Murzakhanov, F. F.; Gabbasov, B. F.; Petrakova, N. V.; Fosca, M.; Barinov, S. M.; Vadalà, G.; Uskoković, V.; Zheng, Y.; Rau, J. V. Antibacterial and Cell-Friendly Copper-Substituted Tricalcium Phosphate Ceramics for Biomedical Implant Applications. *Mater. Sci. Eng., C* **2021**, *129*, 112410.

(4) De Pieri, A.; Rochev, Y.; Zeugolis, D. I. Scaffold-Free Cell-Based Tissue Engineering Therapies: Advances, Shortfalls and Forecast. *npj Regener. Med.* **2021**, *6* (1), 18.

(5) Lorusso, F.; Inchingolo, F.; Dipalma, G.; Postiglione, F.; Fulle, S.; Scarano, A. Synthetic Scaffold/Dental Pulp Stem Cell (DPSC) Tissue Engineering Constructs for Bone Defect Treatment: An Animal Studies Literature Review. *Int. J. Mol. Sci.* **2020**, *21* (24), 9765.

(6) Trivedi, S.; Srivastava, K.; Saluja, T. S.; Shyam, H.; Kumar, S.; Singh, A.; Saxena, S. K.; Mehrotra, D.; Singh, S. K. Hydroxyapatite-Collagen Augments Osteogenic Differentiation of Dental Pulp Stem Cells. *Odontology* **2020**, *108* (2), 251−259.

(7) Ma, L.; Yu, Y.; Liu, H.; Sun, W.; Lin, Z.; Liu, C.; Miao, L. Berberine-Releasing Electrospun Scaffold Induces Osteogenic Differentiation of DPSCs and Accelerates Bone Repair. *Sci. Rep.* **2021**, *11* (1), 1027.

(8) Hagar, M. N.; Yazid, F.; Luchman, N. A.; Ariffin, S. H. Z.; Wahab, R. M. A. Comparative Evaluation of Osteogenic Differentiation Potential of Stem Cells Derived from Dental Pulp and Exfoliated Deciduous Teeth Cultured over Granular Hydroxyapatite Based Scaffold. *BMC Oral Health* **2021**, *21* (1), 263.

(9) Habraken, W.; Habibovic, P.; Epple, M.; Bohner, M. Calcium Phosphates in Biomedical Applications: Materials for the Future? *Mater. Today* **2016**, *19* (2), 69−87.

(10) Dorozhkin, S. V. Nanosized and Nanocrystalline Calcium Orthophosphates. *Acta Biomater.* **2010**, *6* (3), 715−734.

(11) Ignjatovic, N. L.; Ajdukovic, Z. R.; Savic, V. P.; Uskokovic, D. P. Size Effect of Calcium Phosphate Coated with Poly-DL-lactide-*co*-glycolide on Healing Processes in Bone Reconstruction. *J. Biomed. Mater. Res.* **2010**, *94B* (1), 108−117.

(12) Mushtaq, A.; Zhao, R.; Luo, D.; Dempsey, E.; Wang, X.; Iqbal, M. Z.; Kong, X. Magnetic Hydroxyapatite Nanocomposites: The Advances from Synthesis to Biomedical Applications. *Mater. Des.* **2021**, *197*, 109269.

(13) Ignjatović, N.; Wu, V.; Ajduković, Z.; Mihajilov-Krstev, T.; Uskoković, V.; Uskoković, D. Chitosan-PLGA Polymer Blends as Coatings for Hydroxyapatite Nanoparticles and Their Effect on Antimicrobial Properties, Osteoconductivity and Regeneration of Osseous Tissues. *Mater. Sci. Eng., C* **2016**, *60*, 357−364.

(14) Uskoković, V.; Uskoković, D. P. Nanosized Hydroxyapatite and Other Calcium Phosphates: Chemistry of Formation and Application as Drug and Gene Delivery Agents. *J. Biomed. Mater. Res. Part B* **2011**, *96B* (1), 152−191.

(15) Lamkhao, S.; Phaya, M.; Jansakun, C.; Chandet, N.; Thongkorn, K.; Rujijanagul, G.; Bangrak, P.; Randorn, C. Synthesis of Hydroxyapatite with Antibacterial Properties Using a Microwave-Assisted Combustion Method. *Sci. Rep.* **2019**, *9* (1), 4015.

(16) Alipour, M.; Firouzi, N.; Aghazadeh, Z.; Samiei, M.; Montazersaheb, S.; Khoshfetrat, A. B.; Aghazadeh, M. The Osteogenic Differentiation of Human Dental Pulp Stem Cells in Alginate-Gelatin/Nano-Hydroxyapatite Microcapsules. *BMC Biotechnol.* **2021**, *21* (1), 6.

(17) Lin, L.; Chow, K. L.; Leng, Y. Study of Hydroxyapatite Osteoinductivity with an Osteogenic Differentiation of Mesenchymal Stem Cells. *J. Biomed. Mater. Res. Part A* **2009**, *89A* (2), 326−335.

(18) Yang, X.; Li, Y.; Liu, X.; Zhang, R.; Feng, Q. In Vitro Uptake of Hydroxyapatite Nanoparticles and Their Effect on Osteogenic Differentiation of Human Mesenchymal Stem Cells. *Stem Cells Int.* **2018**, *2018*, 1−10.

(19) Uskoković, V.; Wu, V. M. When Nothing Turns Itself Inside out and Becomes Something: Coating Poly(Lactic-Co-Glycolic Acid) Spheres with Hydroxyapatite Nanoparticles vs. the Other Way Around. *J. Funct. Biomater.* **2022**, *13* (3), 102.

(20) Iconaru, S.; Motelica-Heino, M.; Guegan, R.; Beuran, M.; Costescu, A.; Predoi, D. Adsorption of Pb (II) Ions onto Hydroxyapatite Nanopowders in Aqueous Solutions. *Materials* **2018**, *11* (11), 2204.

(21) Uskoković, V. Ion-Doped Hydroxyapatite: An Impasse or the Road to Follow? *Ceram. Int.* **2020**, *46* (8), 11443−11465.

(22) Reger, N. C.; Bhargava, A. K.; Ratha, I.; Kundu, B.; Balla, V. K. Structural and Phase Analysis of Multi-Ion Doped Hydroxyapatite for Biomedical Applications. *Ceram. Int.* **2019**, *45* (1), 252−263.

(23) Evis, Z.; Webster, T. J. Nanosize Hydroxyapatite: Doping with Various Ions. *Adv. Appl. Ceram.* **2011**, *110* (5), 311−321.

(24) Sprio, S.; Dapporto, M.; Preti, L.; Mazzoni, E.; Iaquinta, M. R.; Martini, F.; Tognon, M.; Pugno, N. M.; Restivo, E.; Visai, L.; Tampieri, A. Enhancement of the Biological and Mechanical Performances of Sintered Hydroxyapatite by Multiple Ions Doping. *Front. Mater.* **2020**, *7*..

(25) Ignjatović, N.; Ajduković, Z.; Savić, V.; Najman, S.; Mihailović, D.; Vasiljević, P.; Stojanović, Z.; Uskoković, V.; Uskoković, D. Nanoparticles of Cobalt-Substituted Hydroxyapatite in Regeneration of Mandibular Osteoporotic Bones. *J. Mater. Sci.: Mater. Med.* **2013**, *24* (2), 343−354.

(26) Ignjatović, N. L.; Mančić, L.; Vuković, M.; Stojanović, Z.; Nikolić, M. G.; Škapin, S.; Jovanović, S.; Veselinović, L.; Uskoković, V.; Lazić, S.; Marković, S.; Lazarević, M. M.; Uskoković, D. P. Rare-Earth (Gd3+,Yb3+/Tm3+, Eu3+) Co-Doped Hydroxyapatite as Magnetic, up-Conversion and down-Conversion Materials for Multimodal Imaging. *Sci. Rep.* **2019**, *9* (1), 16305.

(27) Zantye, P.; Fernandes, F.; Ramanan, S. R.; Kowshik, M. Rare Earth Doped Hydroxyapatite Nanoparticles for In Vitro Bioimaging Applications. *Curr. Phys. Chem.* **2019**, *9* (2), 94−109.

(28) Uskoković, V.; Ignjatović, N.; Škapin, S.; Uskoković, D. P. Germanium-Doped Hydroxyapatite: Synthesis and Characterization of a New Substituted Apatite. *Ceram. Int.* **2022**, *48* (19), 27693−27702.

https://doi.org/10.1021/acsanm.3c05974
ACS Appl. Nano Mater. XXXX, XXX, XXX−XXX

(29) Germanium—Element information, properties and uses | Periodic Table. https://www.rsc.org/periodic-table/element/32/germanium (accessed Feb 07, 2023).
(30) Cho, J. M.; Chae, J.; Jeong, S. R.; Moon, M. J.; Shin, D. Y.; Lee, J. H. Immune Activation of Bio-Germanium in a Randomized, Double-Blind, Placebo-Controlled Clinical Trial with 130 Human Subjects: Therapeutic Opportunities from New Insights. *PLoS One* **2020**, *15* (10), No. e0240358.
(31) Vukovic, M.; Lazarevic, M.; Mitic, D.; Jaksic Karisik, M.; Ilic, B.; Andric, M.; Jevtic, B.; Roganovic, J.; Milasin, J. Acetylsalicylic-Acid (ASA) Regulation of Osteo/Odontogenic Differentiation and Proliferation of Human Dental Pulp Stem Cells (DPSCs) in Vitro. *Arch. Oral Biol.* **2022**, *144*, 105564.
(32) Lazarevic, M.; Petrovic, S.; Pierfelice, T. V.; Ignjatovic, N.; Piattelli, A.; Vlajic Tovilovic, T.; Radunovic, M. Antimicrobial and Osteogenic Effects of Collagen Membrane Decorated with Chitosan-Nano-Hydroxyapatite. *Biomolecules* **2023**, *13* (4), 579.
(33) Zucker, R. M.; Massaro, E. J.; Sanders, K. M.; Degn, L. L.; Boyes, W. K. Detection of TiO $_2$ Nanoparticles in Cells by Flow Cytometry. *Cytometry Pt A* **2010**, *77A* (7), 677−685.
(34) Livak, K. J.; Schmittgen, T. D. Analysis of Relative Gene Expression Data Using Real-Time Quantitative PCR and the 2-ΔΔCT Method. *Methods* **2001**, *25* (4), 402−408.
(35) Bumah, V. V.; Masson-Meyers, D. S.; Enwemeka, C. S. Pulsed 450 Nm Blue Light Suppresses MRSA and Propionibacterium Acnes in Planktonic Cultures and Bacterial Biofilms. *J. Photochem. Photobiol., B* **2020**, *202*, 111702.
(36) Pochampally, R. Colony Forming Unit Assays for MSCs. In *Mesenchymal Stem Cells*; Prockop, D. J., Bunnell, B. A., Phinney, D. G., Eds.; Humana Press: Totowa, NJ, 2008; pp 83−91..
(37) Yang, X.; Li, Y.; Liu, X.; Huang, Q.; He, W.; Zhang, R.; Feng, Q.; Benayahu, D. The Stimulatory Effect of Silica Nanoparticles on Osteogenic Differentiation of Human Mesenchymal Stem Cells. *Biomed. Mater.* **2016**, *12* (1), 015001.
(38) Komori, T. Regulation of Proliferation, Differentiation and Functions of Osteoblasts by Runx2. *Int. J. Mol. Sci.* **2019**, *20* (7), 1694.
(39) Tsao, Y.-T.; Huang, Y.-J.; Wu, H.-H.; Liu, Y.-A.; Liu, Y.-S.; Lee, O. Osteocalcin Mediates Biomineralization during Osteogenic Maturation in Human Mesenchymal Stromal Cells. *Int. J. Mol. Sci.* **2017**, *18* (1), 159.
(40) Zan, X.; Sitasuwan, P.; Feng, S.; Wang, Q. Effect of Roughness on in Situ Biomineralized CaP-Collagen Coating on the Osteogenesis of Mesenchymal Stem Cells. *Langmuir* **2016**, *32* (7), 1808−1817.
(41) Lin, G. L.; Hankenson, K. D. Integration of BMP, Wnt, and Notch Signaling Pathways in Osteoblast Differentiation. *J. Cell. Biochem.* **2011**, *112* (12), 3491−3501.
(42) Ponzetti, M.; Rucci, N. Osteoblast Differentiation and Signaling: Established Concepts and Emerging Topics. *Int. J. Mol. Sci.* **2021**, *22* (13), 6651.
(43) Liu, Y.; Wang, G.; Cai, Y.; Ji, H.; Zhou, G.; Zhao, X.; Tang, R.; Zhang, M. In Vitro Effects of Nanophase Hydroxyapatite Particles on Proliferation and Osteogenic Differentiation of Bone Marrow-Derived Mesenchymal Stem Cells. *J. Biomed. Mater. Res. Part A* **2009**, *90A* (4), 1083−1091.
(44) Wang, J.; Yang, G.; Wang, Y.; Du, Y.; Liu, H.; Zhu, Y.; Mao, C.; Zhang, S. Chimeric Protein Template-Induced Shape Control of Bone Mineral Nanoparticles and Its Impact on Mesenchymal Stem Cell Fate. *Biomacromolecules* **2015**, *16* (7), 1987−1996.
(45) Zakaria, S. M.; Sharif Zein, S. H.; Othman, M. R.; Yang, F.; Jansen, J. A. Nanophase Hydroxyapatite as a Biomaterial in Advanced Hard Tissue Engineering: A Review. *Tissue Eng. Part B* **2013**, *19* (5), 431−441.
(46) Uskoković, V.; Desai, T. A. Does Translational Symmetry Matter on the Micro Scale? Fibroblastic and Osteoblastic Interactions with the Topographically Distinct Poly(ε-Caprolactone)/Hydroxyapatite Thin Films. *ACS Appl. Mater. Interfaces* **2014**, *6* (15), 13209−13220.
(47) Wu, V. M.; Ahmed, M. K.; Mostafa, M. S.; Uskoković, V. Empirical and Theoretical Insights into the Structural Effects of Selenite Doping in Hydroxyapatite and the Ensuing Inhibition of Osteoclasts. *Mater. Sci. Eng., C* **2020**, *117*, 111257.
(48) Uskoković, V. Blowup of Accidental Images as a Passageway to Discovery: Insights into the Interaction between Hydroxyapatite Nanoparticles and Human Mesenchymal Stem Cells. *Appl. Sci.* **2020**, *10* (22), 8204.
(49) Ibuki, Y.; Toyooka, T. Nanoparticle Uptake Measured by Flow Cytometry. In *Nanotoxicity. Methods in Molecular Biology*; Reineke, J., Ed.; Humana Press: Totowa, NJ, 2012; Vol. *926*, pp 157−166.
(50) Chen, L.; Mccrate, J. M.; Lee, J. C.-M.; Li, H. The Role of Surface Charge on the Uptake and Biocompatibility of Hydroxyapatite Nanoparticles with Osteoblast Cells. *Nanotechnology* **2011**, *22* (10), 105708.
(51) Cho, E. C.; Zhang, Q.; Xia, Y. The Effect of Sedimentation and Diffusion on Cellular Uptake of Gold Nanoparticles. *Nat. Nanotechnol.* **2011**, *6* (6), 385−391.
(52) Remya, N. S.; Syama, S.; Gayathri, V.; Varma, H. K.; Mohanan, P. V. An in Vitro Study on the Interaction of Hydroxyapatite Nanoparticles and Bone Marrow Mesenchymal Stem Cells for Assessing the Toxicological Behaviour. *Colloids Surf., B* **2014**, *117*, 389−397.
(53) Müller, K. H.; Motskin, M.; Philpott, A. J.; Routh, A. F.; Shanahan, C. M.; Duer, M. J.; Skepper, J. N. The Effect of Particle Agglomeration on the Formation of a Surface-Connected Compartment Induced by Hydroxyapatite Nanoparticles in Human Monocyte-Derived Macrophages. *Biomaterials* **2014**, *35* (3), 1074−1088.
(54) Meena, R.; Kesari, K. K.; Rani, M.; Paulraj, R. Effects of Hydroxyapatite Nanoparticles on Proliferation and Apoptosis of Human Breast Cancer Cells (MCF-7). *J. Nanopart. Res.* **2012**, *14* (2), 712.
(55) Motskin, M.; Wright, D. M.; Muller, K.; Kyle, N.; Gard, T. G.; Porter, A. E.; Skepper, J. N. Hydroxyapatite Nano and Microparticles: Correlation of Particle Properties with Cytotoxicity and Biostability. *Biomaterials* **2009**, *30* (19), 3307−3317.
(56) He, C.; Hu, Y.; Yin, L.; Tang, C.; Yin, C. Effects of Particle Size and Surface Charge on Cellular Uptake and Biodistribution of Polymeric Nanoparticles. *Biomaterials* **2010**, *31* (13), 3657−3666.
(57) Liu, Z.; Xiao, Y.; Chen, W.; Wang, Y.; Wang, B.; Wang, G.; Xu, X.; Tang, R. Calcium Phosphate Nanoparticles Primarily Induce Cell Necrosis through Lysosomal Rupture: The Origination of Material Cytotoxicity. *J. Mater. Chem. B* **2014**, *2* (22), 3480−3489.
(58) Wu, V. M.; Tang, S.; Uskoković, V. Calcium Phosphate Nanoparticles as Intrinsic Inorganic Antimicrobials: The Antibacterial Effect. *ACS Appl. Mater. Interfaces* **2018**, *10* (40), 34013−34028.
(59) Uskoković, V.; Tang, S.; Nikolić, M. G.; Marković, S.; Wu, V. M. Calcium Phosphate Nanoparticles as Intrinsic Inorganic Antimicrobials: In Search of the Key Particle Property. *Biointerphases* **2019**, *14* (3), 031001.
(60) Wu, V. M.; Huynh, E.; Tang, S.; Uskoković, V. Calcium Phosphate Nanoparticles as Intrinsic Inorganic Antimicrobials: Mechanism of Action. *Biomed. Mater.* **2021**, *16* (1), 015018.

https://doi.org/10.1021/acsanm.3c05974
ACS Appl. Nano Mater. XXXX, XXX, XXX−XXX